Large impact basins on Mercury: Global distribution, characteristics, and modification history from MESSENGER orbital data

Caleb I. Fassett[1], James W. Head[2], David M. H. Baker[2], Maria T. Zuber[3], David E. Smith[3,4], Gregory A. Neumann[4], Sean C. Solomon[5], Christian Klimczak[5], Robert G. Strom[6], Clark R. Chapman[7], Louise M. Prockter[8], Roger J. Phillips[7], Jürgen Oberst[9], Frank Preusker[9]

[1]Department of Astronomy, Mount Holyoke College, South Hadley, Massachusetts, USA.
[2]Department of Geological Sciences, Brown University, Providence, Rhode Island, USA.
[3]Department of Earth, Atmospheric, and Planetary Sciences, Massachusetts Institute of Technology, Cambridge, Massachusetts, USA.
[4]NASA Goddard Space Flight Center, Greenbelt, Maryland, USA.
[5]Department of Terrestrial Magnetism, Carnegie Institution of Washington, Washington, D.C., USA.
[6]Lunar and Planetary Laboratory, University of Arizona, Tucson, Arizona, USA.
[7]Department of Space Sciences, Southwest Research Institute, Boulder, Colorado, USA.
[8]The Johns Hopkins University Applied Physics Laboratory, Laurel, Maryland, USA.
[9]Institute of Planetary Research, German Aerospace Center, Berlin, Germany.

For submission to *JGR Planets Special Section on MESSENGER*

v.17

June 4, 2012

Abstract

The formation of large impact basins (diameter $D \geq 300$ km) was an important process in the early evolution of Mercury and influenced the planet's topography, stratigraphy, and crustal structure. We catalog and characterize this basin population on Mercury from global observations by the MESSENGER spacecraft, and we use the new data to evaluate basins suggested on the basis of the Mariner 10 flybys. Forty-two certain or probable impact basins are recognized; a few additional basins that may have been degraded to the point of ambiguity are plausible on the basis of new data but are classified as uncertain. The spatial density of large basins ($D \geq 500$ km) on Mercury is lower than that on the Moon. Morphological characteristics of basins on Mercury suggest that on average they are more degraded than lunar basins. These observations are consistent with more efficient modification, degradation, and obliteration of the largest basins on Mercury than on the Moon. This distinction may be a result of differences in the basin formation process (producing fewer rings), greater relaxation of topography after basin formation (subduing relief), and/or higher rates of volcanism during the period of heavy bombardment on Mercury compared to the Moon (burying basin rings and interiors).

1. Introduction

The importance of impact craters and basins in the geologic evolution of Mercury was apparent on the basis of the first Mariner 10 images and earliest geological mapping [e.g., *Murray et al.*, 1974; *Trask and Guest,* 1975]. The initial studies of Mercury were based on the premise that its cratering record is similar to that of the Moon, although later examination of Mariner 10 data suggested a variety of important differences: (1) There is a deficiency in the density of craters less than ~40–50 km in diameter on Mercury compared with the Moon, even in

57 heavily cratered terrain [*Strom*, 1977; *Strom and Neukum*, 1988]. (2) Secondary craters are more
58 numerous and prominent on Mercury [*Gault et al.*, 1975; *Scott*, 1977; *Spudis and Guest*, 1988].
59 (3) There is a higher average crater density observed on the smooth plains of Mercury than on
60 the lunar maria, as well as less variation in the crater density on plains surfaces on Mercury.
61 This observation has been interpreted to indicate that widespread volcanism terminated earlier on
62 Mercury than the Moon and may have occurred in a more punctuated manner [*Basaltic*
63 *Volcanism Study Project,* 1981; *Spudis and Guest,* 1988; *Strom and Neukum,* 1988]. (4) There is
64 a possible deficiency in the density of large basins on Mercury relative to the Moon [*Malin*,
65 1976; *Wood and Head*, 1976; *Schaber et al.*, 1977; *Frey and Lowry*, 1979], although this
66 inference was disputed by *Spudis and Strobell* [1984] and *Spudis and Guest* [1988], and the
67 discussion was complicated by the fact that different workers used different diameter cutoffs
68 when considering this possible deficiency.
69 The new observations provided by the MErcury Surface, Space ENvironment,
70 GEochemistry, and Ranging (MESSENGER) spacecraft [*Solomon et al*., 2001] have prompted
71 fresh examinations of the cratering record of Mercury and have provided a chance to test earlier
72 hypotheses with more global data [e.g., *Strom et al.*, 2008, 2011; *Fassett et al.*, 2011]. New
73 results strongly support the idea that even in heavily cratered terrains on Mercury, fewer craters
74 are observed than on the lunar highlands for craters with diameter D = 20 to ~128 km [*Fassett et*
75 *al.*, 2011; *Strom et al.*, 2011]. The greater influence of secondary craters on Mercury's cratering
76 record is also supported by new data as well [*Strom et al.*, 2008, 2011; *Chapman et al.*, 2011]. In
77 addition, MESSENGER observations appear to be consistent with the interpretation that there is
78 a limited range in the crater density on the areally extensive smooth plains, particularly since the
79 two largest regions of smooth plains (within and around Caloris, and at high northern latitudes)

have similar superposed crater size-frequency distributions [*Head et al*., 2011; *Ostrach et al.*, 2011].

Although peak-ring basins have been analyzed globally on Mercury [*Baker et al.*, 2011; 2012], the population of the largest basins on Mercury and its similarity to and differences from the corresponding lunar basin population has yet to be thoroughly examined with MESSENGER data and is the major focus of this study. In this paper, we (1) re-examine the basins suggested on the basis of earlier datasets, especially Mariner 10 data, (2) document additional basins from the global orbital observations of Mercury by MESSENGER, (3) assess the size-frequency distribution of basins on Mercury from these global observations and compare it with that of the Moon, (4) analyze the characteristics and modification history of basins on Mercury, and (5) briefly explore the interactions on Mercury among volcanism, tectonics, and basin evolution.

2. Data and Methodology

The primary data for this study are images and derived topography from MESSENGER's Mercury Dual Imaging System (MDIS) [*Hawkins et al.*, 2007] and altimetric data of the northern hemisphere from the Mercury Laser Altimeter (MLA) [*Cavanaugh et al.*, 2007]. Images from the first solar day of MESSENGER's orbital operations provide nearly global coverage with imaging conditions optimized for morphology. These images have been mosaicked into a 250 m/pixel global dataset that we used as the base map for our study. Additional mosaics and individual images from Mariner 10 and MESSENGER were examined where they provided additional coverage or were necessary to assess earlier interpretations. All data were imported and analyzed in the ESRI ArcMap geographic information system (GIS) environment with a Mercury datum of 2440 km radius. The *CraterTools* extension to ArcMap [*Kneissl et al.*, 2010] was used to derive best-fit circles to the basin rims and to measure basin diameters.

105 Basins were mapped systematically by repeated surveying of the MESSENGER image
106 basemap at 1:5 million scale, zooming in as necessary to test the existence of candidate features.
107 Several of the co-authors independently examined the entire dataset. We also specifically re-
108 examined basins suggested in earlier studies, most of which were based on Mariner 10 data
109 [*Murray et al.*, 1974; *Malin*, 1976; *Wood and Head*, 1976; *Schaber et al.*, 1977; *Frey and Lowry*,
110 1979; *Spudis and Guest,* 1988]. A few additional basins were suggested on the basis of radar
111 [*Butler et al.*, 1993] and telescopic studies [*Ksanfomality,* 2004*,* 2008, 2009, 2011; *Ksanfomality*
112 *and Sprague*, 2007].
113 For both the previously suggested and newly mapped basins, a qualitative confidence for the
114 basin was assigned on the basis of the completeness of the basin rim and rim crest, as well as the
115 presence or absence of additional evidence for a basin, such as ejecta, structure, or topography.
116 Basins were classified as certain, probable (Table 1), or suggested/unverified (Table 2). All
117 certain features have a distinctive rim around at least 50% of the basin circumference; probable
118 basins may be less than 50% encircled by a rim, or have other degradation that makes their status
119 less certain. However, these assignments are conservative in that we believe that all certain
120 basins have been correctly classified as impact features and their size estimates and locations are
121 well determined. Most probable basins are also likely to be impact features, but for some their
122 center location or size is uncertain. Basins classified as suggested/unverified are ambiguous;
123 many were suggested on the basis of Mariner 10 or Earth-based telescopic data, and more
124 complete, higher-resolution image coverage and altimetry data from MESSENGER now show
125 that are not likely to be major impact features. However, some basins in this category may be
126 impact structures at a highly degraded state of preservation, and these candidates for the most
127 ancient basins are specifically noted in Table 2. For convenience, basins not assigned names in

128 the prior literature are listed in Tables 1 and 2 with alphanumerical identifiers (e.g., b1, b2, b3) in
129 arbitrary order.
130 Peak-ring and medium-sized basins on Mercury have been recently examined by *Baker et al.*
131 [2011] and *Prockter et al.* [2012]. Only the two largest peak-ring basins described by *Baker et*
132 *al.* [2011] overlap with the size range of the basins considered here.
133
134 **3. Results**
135 **3.1. Density and Size-Frequency Distribution of Certain and Probable Basins on Mercury**
136 We identified 42 certain or probable basins on Mercury; their sizes and locations are
137 provided in Table 1 and Figure 1. This number n of basins with $D \geq 300$ km is only ~35% more
138 than documented on the Moon ($n = 31$) with similar recognition criteria [*Fassett et al.*, 2012],
139 despite Mercury having twice the surface area. The spatial density of basins with $D \geq 300$ km
140 normalized to an area of 10^6 km^2, $N_{Mercury}(300)$, is 0.56 ± 0.09 (where the cited error is $\pm\sqrt{n}/A$, n
141 is number of basins, and A is the measurement area). This density is less than on the Moon,
142 where $N_{Moon}(300) = 0.82 \pm 0.15$.
143 However, closer examination reveals that this difference is entirely the result of a difference
144 in the density of basins with $D \geq 500$ km, because $N_{Mercury}(500) = 0.\ 21 \pm 0.05$ and $N_{Moon}(500) =$
145 0.37 ± 0.1. Figure 2, an R-plot of the full size-frequency distribution of Mercury and the Moon
146 for craters with diameters 20 km and larger, updated with orbital data, illustrates this difference
147 for the largest basins. For large craters and small basins (D = 128-512 km), in contrast, the
148 density between the two bodies is the same within error: $N_{Mercury}(128) - N_{Mercury}(512) = 4.1 \pm 0.2$
149 and $N_{Moon}(128) - N_{Moon}(512) = 3.9 \pm 0.3$ [see also *Fassett et al.*, 2011].
150

151 **3.2. Basins Discovered with MESSENGER Orbital Data**

152 Although a detailed description of the geology of the newly recognized 720-km-diameter
153 Rembrandt impact has been presented earlier [*Watters et al.*, 2009a], many of the other basins
154 that have been seen for the first time in MESSENGER data have yet to be described. Here, we
155 present brief observations of some of these basins.

156 **3.2.1. 730-km-diameter basin (b36) at 7.6°S, 21.6°E**

157 A 730 km in diameter basin, classified as certain, is centered at 7.6°S, 21.6°E (Figure 3). In
158 a few places near the rim, there are possible examples of radial troughs formed by basin ejecta.
159 More prominent sculptured troughs or secondary chains from this basin are found 400 km to its
160 south (26°S, 22°E).

161 The eastern rim and much of the basin interior are superposed by four peak-ring basins
162 [*Baker et al.*, 2011], the youngest of which is Derain [e.g., *Prockter et al.*, 2012] (white arrow,
163 Figure 3). Derain has several anomalous characteristics: between its interior peak ring and
164 exterior rim, it has an exposure of low-reflectance material (LRM) dissimilar from its
165 surroundings [*Robinson et al.,* 2008; *Denevi et al.*, 2009], and its peak ring has been partially
166 removed [*Prockter et al.*, 2012], forming what appear to be hollows [*Blewett et al.*, 2011]. Both
167 hollow formation and LRM exposure within Derain may have been favored in this location
168 because of the pre-existing excavation of material from depth that occurred during formation of
169 the larger, underlying basin. The association of LRM with basins such as Tolstoj and more
170 generally with excavation of materials from depth has been noted earlier [*Robinson et al.,* 2008*;*
171 *Denevi et al.,* 2009].

172 No interior rings of this basin are apparent, although even if interior rings were once present,
173 they may have been destroyed and/or buried by the formation of the numerous superposed

craters and smaller basins. Lobate scarps are localized near the rim in the southwestern part of the basin, where basin-interior materials have been thrust toward the rim (bordered arrow in Figure 3). These scarps are similar to low-relief scarps that have been noted within Beethoven [*André et al*., 2005; *Preusker et al*., 2012]. Localization of contractional deformation involving material thrust away from the basin center is common within large basins on Mercury [*Watters et al.*, 2012].

3.2.2. 470-km-diameter basin (b33) at 72.9°S, 149.9°E

A degraded 470-km-diameter basin classified as probable (Figure 4) was recognized in near-terminator images acquired during a campaign to evaluate the illumination conditions near Mercury's south pole [e.g., *Chabot et al.*, 2012]. Approximately one-quarter of the basin rim is well preserved in its southwestern quadrant (white arrows, Figure 4). The basin is floored by smooth plains that are distinctly smoother than the surrounding, more heavily cratered terrain. In some areas, embayment relations are obscured by subsequently formed secondary crater chains (Figure 4; two white arrows on the left), but many distinctive volcanic embayment relationships [see *Head, et al.,* 2011] are observed (Figure 4; two white arrows on the right). At least two segments of a prominent lobate scarp are localized along the eastern and southern basin rim (bordered arrow, Figure 4), where these interior plains have been thrust toward the rim. This lobate scarp cross-cuts and deforms craters that postdate the interior plains, indicating that contractional deformation occurred after smooth plains emplacement and that the feature cannot be a thick flow front.

3.2.3. 470-km-diameter basin (b38) at 13.4°S, -6.6°E

A relatively well-preserved basin, in the certain category and 470 km in diameter, is centered at 13.4°S, -6.6°E (Figure 5). To its north, northeast, and east this basin has prominent radial

troughs (white arrow, Figure 5), interpreted as sculptured radial ejecta, with widths of 20–25 km and lengths of 100–200 km. The basin rim is non-circular in its eastern sector, with quasi-linear segments that lead to near-perpendicular corners, similar to the eastern rim of Beethoven. Within 100 km of the basin center, young smooth plains embay post-basin craters and are thus stratigraphically separable from the basin itself. The limited extent of the plains may be a result of their confinement within an interior basin ring, although no clear interior rings are observed.

Several chains of secondary craters (~10 km wide) are superposed on the basin interior and are also embayed by the smooth plains. At present, the source of these crater chains is not clear, although the 430-km-diameter basin (b37) immediately to its south, discussed below, is a possible candidate. If these crater chains could be attributed to that basin, then the relative stratigraphy of these two basins, which is presently unclear, could be established.

Outward-facing scarps are present within the basin interior along portions of the rim (bordered arrow, Figure 5), particularly on its southern and eastern sides. As with previous examples, basin interior material has been thrust toward the rim. The scarp on the eastern margin of the basin is notable because it deforms two relatively fresh large craters, 20 km and 40 km in diameter. This relation implies that the most recent episode of thrust faulting in this location occurred well after basin formation and the emplacement of the smooth plains, consistent with relationships between lobate scarps and plains observed in other large basins and elsewhere in this region.

3.2.4. 430-km-basin (b37) at 27.3°S, -3.2°E

Just east of the hilly and lineated terrain [*Murray et al*., 1974], and immediately to the south of the previous example, is a 430-km-diameter basin in the certain category that has two large craters (90 km and 145 km) superposed on its rim (Figure 6). Both of these superposed craters

have smooth plains on their floor, and the basin itself has smooth plains in its interior that completely bury its eastern rim. The eastern rim may have been particularly susceptible to burial due to the superposition of this basin on a degraded large basin to its east (b34 in Table 1), which may have resulted in lower original rim relief to the east. Several craters in excess of 30 km diameter have been superposed on the basin floor and then flooded in their interiors and embayed on their exteriors. These relations suggest that volcanic plains emplacement interior to the basin continued long after the basin formed. No interior rings are observed. Degraded basin ejecta deposits are observed to the northeast of the basin and to its south.

One of the more remarkable features associated with this basin is a lobate scarp more than 200 km long that completely cuts through the smooth floor of the 145-km-diameter crater on its western rim (arrow, Figure 6). The location of this scarp appears to have been controlled by the pre-existing basin structure and follows what would have been the basin rim prior to formation of the 145-km-diameter crater. The fact that this large, outward-facing scarp traces the basin rim despite its location within a younger, large crater suggests that the fault follows a weak zone along the original basin floor and, thus, that it may extend to substantial depth (several tens of kilometers), consistent with models for the depth extent of faulting beneath other large-scale lobate scarps [*Watters et al.*, 2002; *Nimmo and Watters*, 2004]. A similar relationship between a scarp, basin, and younger crater is found in the 130-km-diameter Sayat-Nova crater superposed on the rim of Beethoven basin [*Preusker et al.*, 2012].

3.2.5. 310-km-diameter basin (b40) at 6.5°N, 134.8°E

An example of one of the most heavily modified of the newly identified probable basins is (Figure 7) is a 310-km-diameter structure located ~500 km southwest of the rim of Caloris. Very little of the rim remains intact, except for a small segment on its southern edge. Presently, the

243 basin is outlined by a partial wrinkle-ridge ring. Many other examples of wrinkle-ridge rings
244 have been recognized on Mercury [e.g., *Head et al*., 2008, 2011; *Klimczak et al.*, 2012], but most
245 are smaller in scale. This basin predates Caloris, since material inside its rim is sculptured by
246 Caloris ejecta [e.g., *Fassett et al.*, 2009] (Figure 7, bordered arrow). The plains that presently
247 bury the basin, however, are a portion of the broad expanse of smooth plains exterior to and
248 younger than the Caloris basin. Given the burial and modification state of this basin, it is not
249 surprising that no interior rings or sculptured ejecta outside the basin are observed.
250
251 **3.3. Previously Proposed Basins Not Confirmed by New Data**
252 Previously proposed basins that are uncertain and remain unverified by MESSENGER data
253 are listed in Table 2, along with additional features in the same category seen for the first time in
254 MESSENGER images. Some of these features remain possible, though uncertain, candidates for
255 degraded basins (e.g., Hiroshige-Mahler, Mena-Theophanes). However, all of the basins listed
256 in Table 2 lack strong evidence for a basin interpretation. Most were suggested on the basis of
257 inferred arcs linking tectonic features such as ridges and scarps, which are ubiquitous on
258 Mercury's surface; fitting arcs or circles to these tectonic features thus has the potential to lead to
259 false positives. As an example, some candidate basins (b22, b25) proposed on the basis of near-
260 terminator images obtained during the MESSENGER flybys now appear less likely to be impact
261 features. Instead orbital data have revealed that the postulated rims of these basins are tectonic
262 features, undercutting a basin interpretation.
263 Several workers have argued for the existence of highly degraded basins on the Moon and
264 Mars [e.g., *Frey*, 2011]. As with the lunar examples, candidate basins on Mercury classified
265 here as suggested but unverified are likely to be ancient (pre-Tolstojan) if the impact

interpretation is correct. Basins in this category are predominantly located in heavily cratered terrains and have virtually no topographic expression where data are available. Stratigraphy would also suggest that, if they are basins, they would have to be among the oldest such features in their region. If empirical saturation was reached during the period of heavy bombardment on the Moon and Mercury, as has been argued [e.g., *Fassett et al.*, 2011], then a population of craters and basins degraded to and beyond the limits of recognition is an expected consequence. For this reason, some of the features we classify as suggested but unverified may in fact be the most degraded part of the recognized basin population on the surface of Mercury.

On the other hand, some of the features we have included in this category are not basins. A candidate basin 1000–2000 km in scale named "Skinakas" or "Basin S" was suggested by *Ksanfomality* [2004*,* 2008, 2009] and *Ksanfomality and Sprague* [2007] on the basis of telescopic images of Mercury, as was a nearby feature nicknamed "Medallion" [*Ksanfomality*, 2008, 2009]. MESSENGER images of these proposed basins have been thoroughly evaluated, and no features suggestive of basins are seen at the proposed locations.

Comparison of telescopic images of Mercury with both Mariner 10 and MESSENGER data does suggest that albedo features of approximately ~100–200 km extent and larger are resolvable under prime viewing conditions. In particular, the high-reflectance deposit northeast of Rachmaninoff (~150 km in extent) was clearly imaged by *Dantowitz et al.* [2000]. The classical albedo feature Solitudo Aphrodites [*Dollfus et al.*, 1978] may have contributed to the interpretation by *Ksanfomality* [2004*,* 2008, 2009] of basin "S." However, features smaller than hundreds of kilometers are not resolved from Earth-based telescopic data. The subtle nature and limited topographic expression of many of the basins described here, as well as the substantial

challenges to telescopic imaging of Mercury, underline the difficulty of identifying basins from Earth.

4. Discussion

4.1. Geographic Distribution

The geographic distribution of basins on Mercury (Figure 1) is non-uniform, which may reflect differences either in basin formation or regional resurfacing. The eastern hemisphere (0 to 180°E) has fewer mapped basins (n = 12) than the western hemisphere (-180°E to 0°E) (n = 30). If the impact probability were uniform over the planet, the probability that 30 or more basins out of a total of 42 will be centered in either hemisphere is only 0.8% (note that this binomial probability calculation neglects the fact that basins are spatially extended objects). It is unlikely that the observed difference in the number of basins on the two hemispheres is a result of observational biases. For instance, near-terminator images of the region from 60°E to 120°E, ideal for the recognition of impact features were obtained during the MESSENGER flybys, yet this is the longitude range with the fewest observed basins.

One possible explanation for the dichotomy in the number of observed basins on the two hemispheres is that the impact probability was non-uniform, as would be the case if Mercury were once in synchronous rotation, a situation that can lead to large lateral variations in impact rate [*Wieczorek et al.*, 2012]. The geographic distribution of basins appears consistent with this idea, although additional analysis is necessary to assess the agreement between observations and the expected magnitude of this effect.

Another possible explanation for the hemispheric difference in basin density is that it is a result of differential resurfacing. The distribution of smooth plains that might have buried

311 degraded basins is clearly non-uniform [*Denevi et al*., 2009], as is the distribution of young
312 terrains as determined by crater density [*Fassett et al.*, 2011]. Heterogeneous resurfacing could
313 potentially help account for the lack of recognized basins in a large region to the northwest of
314 Caloris. However, there are broad regions that generally lack both extensive smooth plains and
315 probable-to-certain basins (e.g., at latitudes from 20°N to -65°N and longitudes from 30° to 80°E
316 and from 100° to 145°E).
317
318 **4.2. Basin Topography and Gravity**
319 Topographic data from MLA of Mercury's northern hemisphere [*Zuber et al*., 2012] reveal
320 that the dynamic range of topography (9.85 km) is considerably smaller than that of the Moon
321 (19.9 km) and Mars (30 km). *Zuber et al.* [2012] suggested that part of this difference could be
322 due to the shallow core-mantle boundary of Mercury [*et al.*, 2012] and the possible influence of
323 viscous flow in the mantle and the consequent relaxation of the largest crustal structures, such as
324 the basins we consider here [e.g., *Zhong and Zuber*, 2000; *Mohit et al*., 2009]. Even the
325 topography of the comparatively well-preserved Caloris basin has been substantially modified
326 [*Oberst et al.*, 2010] by processes that led to portions of its interior now standing higher than its
327 rim [*Zuber et al.,* 2012].
328 On Mercury, volcanism appears dominated by emplacement of flood lavas, rather than
329 centralized edifice building [*Head et al.*, 2008, 2009, 2011; *Wilson and Head*, 2008]. Along
330 with the lack of large rift zones, this absence of large edifices may help explain the difference in
331 topographic range. Flood volcanism leads to regional infilling of topographic lows, preferential
332 flooding of crater and basin interiors, and modification of intercrater areas. For example, the
333 contiguous northern volcanic plains on Mercury cover about 6% of the surface, and very few

334 pre-plains crater rims protrude through this deposit, indicating local lava thicknesses in excess of
335 1–2 km [*Head et al.*, 2011]. Such widespread, extensive flooding can readily obscure basin
336 topography at a wide range of scales. Indeed, although the north polar region is a broad lowland,
337 there are only a few probable-to-certain basins in this region (Figure 1b), and additional
338 candidate basins in this area are all degraded to the point of ambiguity.
339 MESSENGER spacecraft tracking data have yielded a model of Mercury's gravity field
340 [*Smith et al.*, 2012]. Prominent positive gravity anomalies in the northern hemisphere are
341 collocated with the Caloris basin and a region near Sobkou, but at the current resolution of the
342 gravity field, most positive anomalies are not clearly associated with mapped impact basins.
343 Combination of the gravity field [*Smith et al.*, 2012] and topography [*Zuber et al.*, 2012] permits
344 the modeling of crustal thickness in Mercury's northern hemisphere. The thinnest crust mapped
345 is beneath the northern lowlands at high northern latitudes, but evidence for a large impact basin
346 there that meets our identification criteria is lacking, perhaps due to flooding and obscuration by
347 subsequent impacts and volcanic plains emplacement [e.g., *Head et al.*, 2011]. Evidence for
348 crustal thinning is seen beneath some impact basins, and Caloris, Sobkou, and Budh meet the
349 criteria for mascons on the basis of evidence for a substantially elevated crust-mantle boundary.
350

351 **4.3. Multiple Rings**
352
353 Multiple (two or more) rings are uncommon in basins ≥ 300 km in diameter on Mercury. The
354 great majority (>80%) of the certain and probable basins we identified have only one
355 physiographically prominent ring that we interpret as the basin rim, often defined by an inward-
356 facing topographic scarp. Both inward of and exterior to this main topographic rim, we typically

357 do not find strong evidence for additional rings, for example at the positions suggested by *Spudis*
358 *and Guest* [1988].

359 This lack of multiple rings is clearly distinct from basins on the Moon, where 52% of basins
360 have at least one interior ring identified with the same criteria as those used here. Even the main
361 rims of basins on Mercury are less commonly intact than for their counterparts on the Moon. A
362 complete or nearly complete rim that encircles more than 75% of the basin is found only for 26%
363 of the basins with $D \geq 300$ km on Mercury, compared with 48% of the basins of the same size on
364 the Moon.

365 An example of a basin with an interior ring is Homer, a large peak-ring basin [*Baker et al*.,
366 2011]. In a few basins, such as Tolstoj and b38 (Figure 5), smooth plains are observed in the
367 central portion of the basin and may be bounded by an interior ring and confined by the resulting
368 basin topography. Likewise, in Beethoven, Rembrandt [*Watters et al.*, 2009a], and Caloris
369 [*Fassett et al.*, 2009], prominent wrinkle ridge rings within the basins may have been localized
370 by interior basin rings.

371 The lack of multiple rings in basins greater than 300 km in diameter of Mercury is surprising,
372 given that peak-ring basins are more common on Mercury than on the Moon or Mars [*Baker et*
373 *al.*, 2011; 2012]. The reason that peak-ring basins have preserved inner rings, whereas larger
374 basins lack inner rings, may be attributable to differences in basin formation, basin modification,
375 or both. For instance, there is substantial evidence that the proportion of impact melt produced
376 during impact events increases with increasing size [e.g., *Cintala and Grieve*, 1998], and so melt
377 production may serve to obscure basin interior structure and ring development in the largest
378 basins. Moreover, relatively more impact melt is thought to result from the higher-velocity

impacts on Mercury, compared with the Moon and other terrestrial planets [*Gault et al*., 1975; *Le Feuvre and Wieczorek*, 2011].

The interior structure of Mercury is known to differ markedly from that of the Moon [e.g., *Smith et al.,* 2012], and this difference could result in differences in the formation of ring structures, such as additional rings beyond the rim crest and peak ring [e.g., *Head*, 2010]. For example, loading of the basin rim and its immediate surroundings by ejecta are enhanced on Mercury relative to the Moon, due to the planet's stronger surface gravitational acceleration [*Gault et al*., 1975]. The combination of this enhanced loading, and the distinct interior and thermal structure of Mercury, could result in early-stage viscous, viscoelastic, or viscoplastic relaxation of basins, in contrast to brittle deformation thought to be responsible for the outer ring and "megaterrace" often seen in large lunar basins [e.g., *Head et al*., 2010]. Immediately after basin formation, the thermal structure of Mercury may have favored the relaxation of basin topographic relief, including the prominence of basin ring structures [e.g., *Mohit et al.*, 2009], as was commonly the case for early lunar basins [*e.g., Baldwin,* 1971; *Solomon et al*., 1982]. Although relaxation by crustal and mantle flow is wavelength-dependent, preferentially favoring the preservation of shorter-wavelength features such as topographic rings, the broad relaxation of topography can enhance the influence of other processes, such as volcanism, in the obliteration of basin structure.

On longer timescales, as described above for specific examples, such processes as the formation of superposed impact craters and basins also serve to obscure basin structure. Moreover, many large basins on Mercury are floored by or covered by plains deposits, and burial of interior rings by volcanism could explain the paucity of interior structures. Extensive burial of

401 basins by volcanism (e.g., Figure 7) may also contribute to the lower percentage of basins on
402 Mercury with a largely intact rim compared with basins on the Moon.
403
404 **4.4. Basin Ejecta and Sculpture**
405 Evidence for radial or sculptured ejecta (e.g., Figure 5) is observed around 29% of the
406 probable or certain basins on Mercury, a figure nearly the same as that for lunar basins in this
407 size range (32%). This fractional similarity is in contrast with the difference in the fraction of
408 basins with well-preserved rims between Mercury and the Moon, an observation suggesting that
409 the interiors of large basins on Mercury may have been more heavily modified than their
410 surroundings.
411
412 **4.5. Basin Formation, Volcanism, and Tectonics**
413 The relationship between basin formation and post-basin volcanism and tectonics provides an
414 important basis for understanding how impact cratering (an exogenic process) and interior
415 (endogenic) processes interact. A few comments related to this topic follow from our survey of
416 the global population of impact basins on Mercury.
417 First, all of the certain or probable basins larger than 300 km in diameter show evidence for
418 superposed smooth or intercrater plains that postdate the basins. Basin b36 (Figure 3) has some
419 of the least evidence for plains in its interior, in large part due to the numerous superposed
420 craters and peak-ring basins. More extensive plains exposures, as are seen in Figures 4-7, are
421 more common. Not only do most basins appear to be at least partially flooded by plains, but
422 initial observations suggest that plains are preferentially located in and around large impact

423 basins. Verifying this relationship will require more complete geological mapping of the surface
424 of Mercury than has been conducted to date.
425 Second, some basins, such as Caloris, Rembrandt, Beethoven, and Sobkou, have sufficiently
426 large exposures of both smooth volcanic plains and basin facies that it is possible to derive
427 independent crater densities for the plains and basins. Current estimates for the density $N(20)$ of
428 impact features at least 20 km in diameter in these four basins are 52 ± 12, 58 ± 16, 68 ± 26, and
429 144 ± 31, respectively. In contrast, the plains within these basins have $N(20)$ values of 23 ± 4, 25
430 ± 10, 44 ± 16, and 22 ± 8, respectively (Figure 8). Thus, the plains are generally appreciably
431 younger than the basins in which they are deposited. This observation provides strong evidence
432 that these interior plains must be volcanic rather than impact melt or ejecta, as has been
433 demonstrated elsewhere on Mercury [e.g., *Head et al.,* 2008, 2009, 2011]. It also suggests that
434 plains emplacement is unlikely to be solely associated with pressure-release melting immediately
435 following the impact [cf. *Elkins-Tanton et al.*, 2004].
436 Third, on the basis of examination of the basins catalogued in this study, post-basin tectonic
437 modification was important as well. Many basins experienced large-scale deformation, mainly
438 along thrust faults that localized near or at the basin margins with units interior to the basins
439 constituting the hanging walls (Figures 3-6). The thrust faults underlying the observed lobate
440 scarps commonly cross-cut younger craters, or deform smooth plains, suggesting that most
441 outward-facing scarps at the margin of basins have a tectonic origin rather than being preserved
442 volcanic flow fronts, although specific exceptions may exist [see Figure 4 and discussion by
443 *Head et al.*, 2011]. The presence of these prominent scarps along or near the basin rim suggests
444 that the localization of contractional deformation on Mercury is favored along weak zones that
445 follow the rims and floors of large impact structures. Further, the age relationships between

446 scarps and both young craters and smooth plains indicate that at least some portion of large-scale
447 thrust faulting postdated volcanic plains emplacement.
448 Wrinkle ridges that are found in smooth plains units also appear to be affected by pre-
449 existing basins (e.g., Figure 7), as is common for smaller craters. In a few instances, evidence of
450 extensional tectonic features is also observed in some large basins, such as Caloris [*Watters et*
451 *al.*, 2005] and Rembrandt [*Watters et al.*, 2009a], although extension is less common than
452 compression, as has been noted elsewhere [e.g., *Watters et al.*, 2009b].
453
454 **4.6. Spatial Density of Basins on Mercury and the Moon**
455 A substantially lower density of large ($D \geq 500$ km) certain or probable basins is observed on
456 Mercury than the Moon. Indeed, the basin population on Mercury would be more similar to the
457 lunar population if all pre-Nectarian basins on the Moon were excluded. There are three broad
458 categories of hypotheses that might explain this difference: (1) An observational effect: The
459 lower density on Mercury might simply be a result of the type or quality of data available for
460 Mercury compared with data for the Moon. (2) A formational effect: Differences in the basin
461 formation process on the two planetary bodies, for instance, might be expressed as a lower
462 density of the largest basins on Mercury (e.g., if growth of the basin cavity or outer ring
463 formation were inhibited or rapidly modified during basin formation on Mercury). Alternatively,
464 a different population of large impactors affecting Mercury from those impacting the Moon
465 might result in fewer large basins. If basins on Mercury have less topographic relief than on the
466 Moon, still another possibility is that they might thereby be more susceptible to modification and
467 obscuration. (3) A later-stage modification effect: After formation, large basins on Mercury
468 might simply have been modified and degraded more efficiently. Relaxation of large basins may

469 have occurred by crustal and mantle flow, followed by emplacement of plains, either due to
470 widespread volcanism unrelated to basin formation, or as a result of volcanism triggered by basin
471 formation.

472 It is unlikely that the difference in the density of large basins can be solely an observational
473 effect. MESSENGER data have provided a global image mosaic with conditions suitable for
474 recognition of impact basins over most of the surface of Mercury. On the basis of data from
475 Mariner 10, the three MESSENGER flybys, and MESSENGER orbital observations, much of the
476 surface has been imaged at multiple illumination geometries. Topography from MLA [*Zuber et*
477 *al.*, 2012] and stereo images [*Preusker et al*., 2011, 2012] provide additional data for recognizing
478 basins.

479 For Mercury to have a lunar-like density of probable-to-certain basins with $D \geq 500$ km
480 basins would require an additional 10-15 features of this size on Mercury. Although a few
481 additional candidates of this size are recognized, the candidate basins in Table 2 are at best
482 uncertain, and most are unlikely to be impact structures. Moreover, the density of probable-to-
483 certain lunar basins given here is conservative, and the Moon also has numerous candidate basins
484 [e.g., *Frey*, 2011] that are similar to the basins in the suggested/unverified class here. Applying a
485 different threshold for basin recognition is thus unlikely to close the observed difference between
486 the two planetary bodies.

487 An explanation for this difference that focuses on basin formation processes is more likely.
488 As described above, there are known differences in parameters that affect crater formation on the
489 Moon and Mercury, such as impact velocity, surface gravitational acceleration, and planetary
490 interior structure, all of which can affect crater growth [e.g., *Schultz,* 1988], collapse [e.g., *Head*,
491 2010], and early modification. Exploring this explanation would require additional modeling of

492 the basin formation process, which could help to better constrain this idea. One option is that the
493 outward growth of basins is inhibited on Mercury compared with the Moon, so that formation of
494 rings equivalent to the Cordillera ring surrounding the lunar Orientale basin [*Head*, 1974, 2010]
495 is less likely. If this were the case, such an effect might lead to a lower density of very large
496 basins on Mercury than the Moon. For example, if 10-15 examples in the population of basins in
497 the 300–500 km diameter range on Mercury had developed a distinctive outer topographic ring
498 that would alter our interpretation of the overall basin size, the discrepancy between the Moon
499 and Mercury (Figure 2) would be reduced or erased without substantially changing the statistics
500 below ~500 km diameter. Currently it is thought that Mercury and the Moon had the same early
501 impactor populations, on the basis of the similarity in the shape of their crater size-frequency
502 distributions [e.g., *Strom et al.*, 2008, 2011; *Fassett et al.*, 2011]. Although vulcanoids could be a
503 distinct reservoir of impactors for Mercury [e.g., *Leake et al.*, 1987], it is not clear how this extra
504 reservoir of impacting objects would yield a situation in which Mercury has fewer large basins
505 than the Moon, particularly with a similar size-frequency distribution and similar density of
506 smaller impact features.
507 Thus, as an explanation of the difference in density of large basins between Mercury and the
508 Moon, we favor a combination of factors, including (1) less ready development of an outer basin
509 ring on Mercury, (2) more extensive early modification of topographic relief for basins on
510 Mercury, and (3) more extensive later modification of the largest basins on Mercury by interior
511 volcanism. Specifically, it appears that volcanism and deformation were more important during
512 the early history of Mercury than during comparable periods on the Moon, and thus more
513 efficient at obscuring and/or obliterating large basins on Mercury than on the lunar surface. On
514 the Moon as well as on Mercury, densities of heavily cratered surfaces are consistent with their

515 having been cratered to saturation equilibrium [e.g., *Fassett et al.,* 2011, and references therein].
516 However, if another process such as volcanism were important for obliterating basins, the
517 expected equilibrium population of basins would be at a lower density than from crater saturation
518 alone [see, e.g., *Chapman and Jones*, 1977]. In the case of Mercury, because impact features in
519 the diameter range D~128-512 km have the same density as on the Moon, modification
520 processes would have to affect larger basins most strongly. Differences in basin collapse stages
521 [e.g., *Head*, 2010] could make large impact basins appear initially smaller and/or less prominent,
522 relaxation by crustal and mantle flow [e.g., *Mohit et al.*, 2009] could preferentially modify larger
523 features, and volcanism linked to the formation of the largest basins [e.g., *Roberts and Barnouin*,
524 2012] could help account for these observations. All basins on Mercury ≥ 300 km in diameter,
525 including features 300–500 km in diameter, show evidence for being at least partially superposed
526 by younger plains, and basins on Mercury have less well-preserved rims and interior rings than
527 those on the Moon. These characteristics point to earlier large basins having been formed,
528 degraded, and buried beyond the point that they can be readily recognized.
529
530
531 **5. Conclusions**
532 MESSENGER data have been used to map and characterize large impact basins on
533 Mercury's surface and to test the existence of previously suggested basins. Our data suggest that
534 there are fewer certain or probable impact basins per unit area on Mercury than on the Moon for
535 basins with diameters larger than 500 km. The basins that are observed on Mercury appear
536 qualitatively more degraded than those on the Moon, with less likelihood to have intact rims or
537 interior rings. These data suggest that initial basin formation processes and early modification

538 processes were different on the two bodies. Moreover, volcanism and other geological processes
539 that degrade large basins over longer timescales were more important on Mercury than on the
540 Moon during the first billion years of solar system history.
541
542 **Acknowledgments**. The Integrated Software for Imagers and Spectrometers (ISIS) software
543 package of the United States Geological Survey was used for data processing in this study. We
544 thank Thomas Kneissl for developing and sharing the CraterTools extension to ArcMap.
545 Mapping by Seth Kadish from MESSENGER flyby data helped contribute to this analysis. The
546 MESSENGER project is supported by NASA Discovery Program through contracts to The Johns
547 Hopkins Applied Physics Laboratory (NAS5-97271) and the Carnegie Institution of Washington
548 (NASW-00002).
549

550 Table 1. Certain and probable impact basins on Mercury, $D \geq 300$ km.

Basin Name / ID	*D*, km	Lat °N	Lon °E	Confidence	Source	Note
Caloris	1550	31.4	160.3	Certain	M10	*Murray et al.* [1974]; SG1
b30	1390	15.9	21.1	Probable	Flyby DEM	*Preusker et al.* [2011]
Matisse-Repin	950	-24.3	-75.6	Certain	M10	SG11
Andal-Coleridge	830	-42.6	-51.0	Probable	M10 / DEM	SG10
Borealis (?)	790	71.0	-81.0	Probable	Orbit	SG14 (?) (relocated)
Sobkou	770	33.4	-133.0	Certain	M10	SG5
b31	770	36.6	3.6	Probable	Flyby DEM	*Preusker et al.* [2011]
b45	770	45.3	43.3	Probable	Orbit	
b36	730	-7.6	21.6	Certain	Orbit	
b34	720	-30.1	6.0	Probable	Orbit DEM	
Rembrandt	720	-33.0	87.8	Certain	Flybys	*Watters et al.* [2009a]
Vincente-Yakovlev	690	-52.6	-162.1	Probable	M10 / DEM	SG12
Budh	680	17.2	-151.7	Probable	M10	SG16
Beethoven	630	-20.8	-123.9	Certain	M10	*Schaber et al.* [1977]
b54	610	-1.8	-59.4	Probable	Orbit DEM	
b12	550	3.7	74.5	Probable	Flybys	
Tolstoj	490	-16.4	-165.1	Certain	M10	*Murray et al.* [1974]; SG2
Hawthorne-Riemenschneider	470	-55.9	-105.9	Probable	M10/DEM	SG18
b33	470	-72.9	149.9	Probable	Orbit	
b38	470	-13.4	-6.6	Certain	Orbit	
b44	450	-10.3	102.6	Probable	Orbit	
b37	430	-27.3	-3.2	Certain	Orbit	
b2	420	-39.0	-101.4	Certain	Flybys	
Dostoevskij	410	-44.5	-176.5	Certain	M10	*Murray et al.* [1974]
Derzhavin-Sor Juana	400	50.2	-26.1	Probable	M10	SG15
b11	390	-2.6	-56.1	Certain	Flybys	
b39	390	-26.5	-142.0	Certain	Orbit	
b27	390	27.9	-158.6	Certain	M10/Orbit	*Murray et al.* [1974]
b32	370	55.8	-10.6	Probable	Flyby DEM	*Preusker et al.* [2011]
Shakespeare	360	48.9	-152.3	Certain	M10	*Murray et al.* [1974]; SG4
b20	360	-3.1	-44.2	Certain	M10	*Murray et al.* [1974]
b52	360	-30.3	153.5	Probable	Orbit	
b41	350	-44.8	-142.7	Probable	Orbit	
b3 (“Chong-Gauguin”?)	330	57.1	-107.9	Certain	M10/Flybys	SG20 (smaller)
Goethe	320	81.4	-54.3	Certain	M10	*Schaber et al.* [1977]
Raphael	320	-20.3	-76.1	Certain	M10	*Schaber et al.* [1977]
b6	320	-17.5	-96.6	Probable	Flybys	
Homer	310	-1.7	-36.8	Certain	M10	*Murray et al.* [1974]
b4	310	28.9	-113.8	Certain	M10	*Schaber et al.* [1977]
b9	310	-25.0	-98.8	Probable	Flybys	
b40	310	6.5	134.8	Probable	Orbit	
Vy-asa	310	49.7	-84.5	Certain	M10	*Schaber et al.* [1977]

551 Note: SG is row number in Table II of *Spudis and Guest* [1988].

552 Table 2. Suggested and unverified impact basins on Mercury, $D \geq 300$ km.

Basin Name / ID	Diameter (km)	Lat (°N)	Lon (°E)	Source	Note
Basin "S"/"Skinakas"	~1000-2000	8	80	Telescopic	*Ksanfomality* [2004]
"Medallion"	~1000	0	60	Telescopic	*Ksanfomality* [2008]
b57	1250	-16	86	Orbit	
Tir	1250	6	-168	M10	SG9
Eitoku-Milton	1180	-23	-171	M10	SG13
Bartok-Ives	1175	-33	-115	M10	SG22
Donne-Moliere	1060	4	-10	M10	SG21
b56*	1020	-18	48	Orbit	
b13	~1000	17	122	Radar	*Butler et al.* [1993]
b14	~1000	55	12	Radar	*Butler et al.* [1993]
b15	~1000	-29	11	Radar	*Butler et al.* [1993]
Sadi-Scopus	930	-82.5	-44	M10	SG23
Mena-Theophanes*	770	-1	-129	M10	SG8
b59*	740	49.5	-120	Orbit	
b16	720	-45.5	137.2	Flybys	
b53	670	-0.6	140.6	Orbit	
Ibsen-Petrarch	640	-31	-30	M10	SG17
Brahms-Zola	620	59	-172	M10	SG6
b50	620	56.3	68.6	Orbit	
b60*	620	83	83	Orbit	
b55*	580	53	-59.8	Orbit	
b43*	540	-1.1	149.5	Orbit	
b58*	530	-62	-140	Orbit	
Gluck-Holbein	500	35	-19	M10	SG19
b1	450	-8	-65	M10	*Malin* [1976]
b25	440	-15	93	Flybys	
b22	400	0	93	Flybys	
b42	400	-12.8	171.2	Orbit	Less than 50% of rim (if it exists)
b51	400	-74.2	-13.8	Orbit	
b5	380	27.3	-146.1	M10	*Schaber et al.* [1977]
b47*	360	23.0	-170.5	Orbit	
b49	360	55.6	-28.9	Orbit	
b61	360	77	-142.5	Orbit	
b62*	360	78.5	166	Orbit	
Hiroshige-Mahler*	355	-16	-23	M10	SG7; MESSENGER data not ideal to test
b18	340	10.8	65.6	Flybys	
b46	320	-40.6	130.2	Orbit	
b48	320	-37.7	-78.7	Orbit	

553
554 Notes: SG is row number in Table II of *Spudis and Guest* [1988]. *Examples of basins that are uncertain or ambiguous,
555 but are possible on the basis of current data. These are the most likely members of this list to be degraded impact
556 structures.
557
558

559
560 **References**
561

562 André, S. L., T. R. Watters, and M. S. Robinson (2005), The long wavelength topography of
563 Beethoven and Tolstoj basins, Mercury, *Geophys. Res. Lett., 32,* L21202,
564 doi:10.1029/2005GL023627.
565 Baker, D. M. H., J. W. Head, S. C. Schon, C. M. Ernst, L. M. Prockter, S. L. Murchie, B. W.
566 Denevi, S. C. Solomon, and R. G. Strom (2011), The transition from complex crater to peak-
567 ring basin on Mercury: New observations from MESSENGER flyby data and constraints on
568 basin formation models, *Planet. Space. Sci.*, *59*, 1932–1948, doi:10.1016/j.pss.2011.05.010.
569 Baker, D. M. H., et al. (2012), New morphometric measurements of peak-ring basins on Mercury
570 and the Moon: Results from the Mercury Laser Altimeter and Lunar Orbiter Laser Altimeter,
571 *Lunar Planet. Sci., 43*, abstract 1238.
572 Baldwin, R. B. (1971), The question of isostasy on the Moon, *Phys. Earth Planet. Inter.*, *4*, 167–
573 179.
574 Basaltic Volcanism Study Project (1981), *Basaltic Volcanism on the Terrestrial Planets.*
575 Pergamon Press, New York, 1286 pp.
576 Blewett, D. T., et al. (2011), Hollows on Mercury: MESSENGER evidence for geologically
577 recent volatile-related activity, *Science*, *333*, 1856–1859, doi: 10.1126/science.1211681.
578 Butler, B. J., D. O. Muhleman, and M. A. Slade (1993), Mercury: Full-disk radar images and the
579 detection and stability of ice at the north pole, *J. Geophys. Res.*, *98*, 15,003–15,023,
580 doi:10.1029/93JE01581.
581 Cavanaugh, J. F., et al. (2007), The Mercury Laser Altimeter instrument for the MESSENGER
582 mission, *Space Sci. Rev.*, *131*, 451–479.
583 Chabot, N. L., C. M. Ernst, B. W. Denevi, J. K. Harmon, S. L. Murchie, D. T. Blewett, S. C.
584 Solomon, and E. D. Zhong (2012), Areas of permanent shadow in Mercury's south polar
585 region, *Geophys. Res. Lett., 39*, L09204, doi:10.1029/2012GL051526.
586 Chapman, C. R., and K. L. Jones (1977), Cratering and obliteration history of Mars, *Ann. Rev.*
587 *Earth Planet. Sci.*, *5*, 515–540.

588 Chapman, C. R., W. J. Merline, L. R. Ostrach, Z. Xiao, S. C. Solomon, J. W. Head, and J. L.
589 Whitten (2011), Statistics of morphologies of small primary and secondary craters on
590 Mercury's northern plains, *Abstracts with Programs, 43* (5), paper 142-13, p. 359, Geological
591 Society of America, Boulder, Colo.
592 Crater Analysis Techniques Working Group (1978), Standard techniques for presentation and
593 analysis of crater size-frequency data, Tech. Memo. 79730, 24 pp., NASA, Washington, D.C.
594 Dantowitz, R. F., S. W. Teare, and M. J. Kozubal (2000), Ground-based high-resolution imaging
595 of Mercury, *Astron. J.*, *119*, 2455–2457.
596 Denevi, B. W., et al. (2009), The evolution of Mercury's crust: A global perspective from
597 MESSENGER, *Science*, *324*, 613–618, doi:10.1126/science.1172226.
598 Elkins-Tanton, L. T., B. H. Hager, and T. L. Grove (2004), Magmatic effects of the lunar late
599 heavy bombardment, *Earth Planet. Sci. Lett., 222*, 17–27, doi:10.1016/j.epsl.2004.02.017.
600 Fassett, C. I., J. W. Head, D. T. Blewett, C. R. Chapman, J. L. Dickson, S. L. Murchie, S. C.
601 Solomon, and T. R. Watters (2009), Caloris impact basin: Exterior geomorphology,
602 stratigraphy, morphometry, radial sculpture, and smooth plains deposits, *Earth Planet. Sci.*
603 *Lett., 285*, 297–308, doi:10.1016/j.epsl.2009.05.022.
604 Fassett, C. I., S. J. Kadish, J. W. Head, S. C. Solomon, and R. G. Strom (2011), The global
605 population of large craters on Mercury and comparison with the Moon, *Geophys. Res. Lett.,*
606 *38*, L10202, doi:10.1029/2011GL047294.
607 Fassett, C. I., J. W. Head, S. J. Kadish, E. Mazarico, G. A. Neumann, D. E. Smith, and M. T.
608 Zuber (2012), Lunar impact basins: Stratigraphy, sequence and ages from superposed impact
609 crater populations measured from Lunar Orbiter Laser Altimeter (LOLA) data, *J. Geophys.*
610 *Res., 117*, E00H06, doi:10.1029/2011JE003951.
611 Frey, H. (2011), Previously unknown large impact basins on the Moon: Implications for lunar
612 stratigraphy, *Special Paper 477*, 53–75, Geological Society of America, Boulder, Colo.,
613 doi:10.1130/2011.2477(02).
614 Frey, H. and B. L. Lowry (1979), Large impact basins on Mercury and relative crater production
615 rates, *Proc. Lunar Planet. Sci. Conf., 10th*, 2669–2687.
616 Gault, D. E., J. E. Guest, J. B. Murray, D. Dzurisin, and M. C. Malin (1975), Some comparisons
617 of impact craters on Mercury and the Moon, *J. Geophys. Res.*, *80*, 2444–2460,
618 doi:10.1029/JB080i017p02444.

619 Harmon, J. K., M. A. Slade, B. J. Butler, J. W. Head, M. S. Rice, and D. B. Campbell (2007),
620 Mercury: Radar images of the equatorial and midlatitude zones, *Icarus*, *187*, 374–405.
621 Hawkins, S. E., II, et al. (2007), The Mercury Dual Imaging System on the MESSENGER
622 spacecraft, *Space Sci. Rev.*, *131*, 247–338, doi:10.1007/s11214-007-9266-3.
623 Head, J. W. (1974), Orientale multi-ringed basin interior and implications for the petrogenesis of
624 lunar highland samples, *Moon*, 11, 327–356.
625 Head, J. W. (2010), Transition from complex craters to multi-ringed basins on terrestrial
626 planetary bodies: Scale-dependent role of the expanding melt cavity and progressive
627 interaction with the displaced zone, *Geophys. Res. Lett.*, 37, L02203,
628 doi:10.1029/2009GL041790.
629 Head, J. W., et al. (2008), Volcanism on Mercury: Evidence from the first MESSENGER flyby,
630 *Science*, *321*, 69–72.
631 Head, J. W., et al. (2009), Volcanism on Mercury: Evidence from the first MESSENGER flyby
632 for extrusive and explosive activity and the volcanic origin of plains, *Earth Planet. Sci. Lett.*,
633 *285*, 227–242, doi:10.1016/j.epsl.2009.03.007.
634 Head, J. W., et al. (2011), Flood volcanism in the northern high latitudes of Mercury revealed by
635 MESSENGER, *Science*, *333*, 1853–1856.
636 Klimczak, C., T. R. Watters, C. M. Ernst, A. M. Freed, P. K. Byrne, S. C. Solomon, D. M. Blair,
637 and J. W. Head, (2012), Deformation associated with ghost craters and basins in volcanic
638 smooth plains on Mercury: Strain analysis and implications for plains evolution, *J. Geophys.*
639 *Res*., submitted.
640 Kneissl, T., S. van Gasselt, and G. Neukum (2010), Map-projection-independent crater size-
641 frequency determination in GIS environments – new software tool for ArcGIS, *Planet. Space*
642 *Sci., 59*, 1243–1254, doi:10.1016/j.pss.2010.03.015.
643 Ksanfomality, L. V. (2004), A huge basin in the unknown portion of Mercury in the 250°–290°
644 W longitude range, *Solar Syst. Res.*, *38*, 21–27.
645 Ksanfomality, L. V. (2008), The surface of Mercury from ground-based astronomical
646 observations, *Solar Syst. Res.*, *42*, 451–472.

647 Ksanfomality, L. V. (2009), The surface of Mercury in the 210–350° W longitude range, *Icarus*,
648 *200*, 367–373.
649 Ksanfomality, L. V. (2011), Study of the unknown hemisphere of Mercury by ground-based
650 astronomical facilities, *Solar Syst. Res.*, *45*, 281–303, doi:10.1134/S0038094611040034.
651 Ksanfomality, L. V., and A. L. Sprague (2007), New images of Mercury's surface from 210° to
652 290° W longitudes with implications for Mercury's global asymmetry, *Icarus*, *188*, 271–287.
653 Leake, M. A., C. R. Chapman, S. J. Weidenschilling, D. R. Davis, and R. Greenberg (1987), The
654 chronology of Mercury's geological and geophysical evolution: The vulcanoid hypothesis,
655 *Icarus, 71,* 350–375.
656 Le Feuvre, M., and M. A. Wieczorek (2011), Nonuniform cratering of the Moon and a revised
657 crater chronology of the inner solar system, *Icarus*, *214*, 1–20.
658 Malin, M. C. (1976), Comparison of large crater and multi-ringed basin populations on Mars,
659 Mercury, and the Moon, *Proc. Lunar Plan. Sci. Conf., 7th*, 3589–3602.
660 Mohit, P. S., C. L. Johnson, O. Barnouin-Jha, M. T. Zuber, and S. C. Solomon (2009), Shallow
661 basins on Mercury: Evidence of relaxation?, *Earth Planet. Sci. Lett.,* 285, 355–363.
662 Murray, B. C., M. J. S. Belton, G. E. Danielson, M. E. Davies, D. E. Gault, B. Hapke, B.
663 O'Leary, R. G. Strom, V. Suomi, and N. Trask (1974), Mercury's surface: Preliminary
664 description and interpretation from Mariner 10 pictures, *Science*, *185*, 169–179.
665 Nimmo, F., and T. R. Watters (2004), Depth of faulting on Mercury: Implications for heat flux
666 and crustal and effective elastic thickness, *Geophys. Res. Lett.*, *31*, L02701,
667 doi:10.1029/2003GL018847.
668 Oberst, J., F. Preusker, R. J. Phillips, T. R. Watters, J. W. Head, M. T. Zuber, and S. C. Solomon
669 (2010), The morphology of Mercury's Caloris basin as seen in MESSENGER stereo
670 topographic models, *Icarus*, *209*, 230–238, doi:10.1016/j.icarus.2010.03.009.
671 Ostrach, L. R., C. R. Chapman, C. I. Fassett, J. W. Head, W. J. Merline, M. S. Robinson, S. C.
672 Solomon, R. G. Strom, and Z. Xiao (2011), Crater statistics for the northern polar region of
673 Mercury derived from MESSENGER orbital data, *Abstracts with Programs, 43* (5), paper
674 142-14, p. 360, Geological Society of America, Boulder, Colo.
675 Pike, R. J. (1988), Geomorphology of impact craters on Mercury, in *Mercury*, edited by F. Vilas,
676 C. R. Chapman, and M. S. Matthews, pp. 165–273, University of Arizona Press, Tucson,
677 Ariz.

678 Preusker, F., J. Oberst, J. W. Head, T. R. Watters, M. S. Robinson, M. T. Zuber, and S. C.
679 Solomon (2011), Stereo topographic models of Mercury after three MESSENGER flybys,
680 *Planet. Space Sci.*, *59*, 1910–1917, doi:10.1016/j.pss.2011.07.005.
681 Preusker, F., J. Oberst, D. T. Blewett, K. Gwinner, J. W. Head, S. L. Murchie, M. S. Robinson,
682 T. R. Watters, M. T. Zuber, and S. C. Solomon (2012), Topography of Mercury from stereo
683 images: First samples from MESSENGER orbital mapping, *Lunar Planet. Sci., 43*, abstract
684 1913.
685 Prockter, L. M., S. L. Murchie, C. M. Ernst, D. M. H. Baker, P. K. Byrne, J. W. Head, T. R.
686 Watters, B. W. Denevi, C. R. Chapman, and S. C. Solomon (2012), The geology of medium-
687 sized basins on Mercury: Implications for surface processes and evolution, *Lunar Planet.*
688 *Sci., 43*, abstract 1326.
689 Roberts, J. H., and O. S. Barnouin (2012), The effect of the Caloris impact on the mantle
690 dynamics and volcanism of Mercury, *J. Geophys. Res.*, *117*, E02007,
691 doi:10.1029/2011JE003876.
692 Robinson, M. S., et al. (2008), Reflectance and color variations on Mercury: Regolith processes
693 and compositional heterogeneity, *Science*, *321*, 66–69, doi:10.1126/science.1160080.
694 Schaber, G. G., J. M. Boyce, and N. J. Trask (1977), Moon–Mercury: Large impact structures,
695 isostasy, and average crustal viscosity, *Phys. Earth Planet. Inter., 15*, 189–201.
696 Schultz, P. H. (1988), Cratering on Mercury: A relook, in *Mercury*, edited by F. Vilas, C. R.
697 Chapman, and M. S. Matthews, pp. 274–335, University of Arizona Press, Tucson, Ariz.
698 Scott, D. H. (1977), Moon–Mercury: Relative preservations state of secondary craters, *Phys.*
699 *Earth Planet. Inter., 15*, 173–178.
700 Smith, D. E., et al. (2012), Gravity field and internal structure of Mercury from MESSENGER,
701 *Science*, *336*, 214–217, doi:10.1126/science.1218809.
702 Solomon, S. C., R. P. Comer, and J. W. Head (1982), The evolution of impact basins: Viscous
703 relaxation of topographic relief, *J. Geophys. Res.*, *87*, 3975–3992.
704 Solomon, S. C., et al. (2001), The MESSENGER mission to Mercury: Scientific objectives and
705 implementation, *Planet. Space Sci., 49,* 1445–1465.
706 Spudis, P. D., and M. E. Strobell (1984), New identification of ancient multi-ring basins on
707 Mercury and implications for geologic evolution, *Lunar Planet. Sci.*, *15,* 814–815.

708 Spudis, P. D., and J. E. Guest (1988), Stratigraphy and geologic history of Mercury, in *Mercury*,
709 edited by F. Vilas, C.R. Chapman, and M.S. Matthews, pp. 118–164, University of Arizona
710 Press, Tucson, Ariz.
711 Strom, R. G. (1977), Origin and relative age of lunar and Mercurian intercrater plains, *Phys.*
712 *Earth Planet. Inter., 15*, 156–172.
713 Strom, R. G., N. J. Trask, and J. E. Guest (1975), Tectonism and volcanism on Mercury, *J.*
714 *Geophys. Res., 80*, 2478–2507.
715 Strom, R. G., R. Malhotra, T. Ito, F. Yoshida, D. A. Kring (2005), The origin of planetary
716 impactors in the inner solar system, *Science, 309*, 1847–1850.
717 Strom, R. G., C. R. Chapman, W. J. Merline, S. C. Solomon, and J. W. Head (2008), Mercury
718 cratering record viewed from MESSENGER's first flyby, *Science*, *321*, 79–81,
719 doi:10.1126/science.1159317.
720 Strom, R. G., M. Banks, C. R. Chapman, C. I. Fassett, J. A. Forde, J. W. Head, W. J. Merline, L.
721 M. Prockter, and S. C. Solomon (2011), Mercury crater statistics from MESSENGER flybys:
722 Implications for stratigraphy and resurfacing history, *Planet. Space Sci*., *59*, 1960–1967.
723 Trask, N. J., and J. E. Guest (1975), Preliminary geologic terrain map of Mercury, *J. Geophys.*
724 *Res.*, *80*, 2461–2477.
725 Watters, T. R., R. A. Schultz, M. S. Robinson, and A. C. Cook (2002), The mechanical and
726 thermal structure of Mercury's early lithosphere, *Geophys. Res. Lett.*, *29*, 1542,
727 doi:10.1029/2001GL014308.
728 Watters, T. R., F. Nimmo, and M. S. Robinson (2005), Extensional troughs in the Caloris basin
729 of Mercury: Evidence of lateral crustal flow, *Geology*, *33*, 669–672.
730 Watters, T. R., J. W. Head, S. C. Solomon, M. S. Robinson, C. R. Chapman, B. W. Denevi, C. I.
731 Fassett, S. L. Murchie, and R. G. Strom (2009a), Evolution of the Rembrandt impact basin on
732 Mercury, *Science*, *324*, 618–621.
733 Watters, T. R., S. C. Solomon, M. S. Robinson, J. W. Head, S. L. André, S. A. Hauck II, and S.
734 L. Murchie (2009b), The tectonics of Mercury: The view after MESSENGER's first flyby,
735 *Earth Planet. Sci. Lett.*, *285*, 283–296, doi:10.1016/j.epsl.2009.01.025.
736 Watters, T. R., S. C. Solomon, M. S. Robinson, J. W. Head, R. G. Strom, C. Klimczak, P. K.
737 Byrne, A. C. Enns, C. M. Ernst, L. M. Prockter, S. L. Murchie, J. Oberst, F. Preusker, M. T.

738 Zuber, S. A. Hauck, II, and R. J. Phillips (2012), Tectonic features on Mercury: An orbital
739 view with MESSENGER, *Lunar Planet. Sci., 43*, abstract 2121.
740 Wieczorek, M. A., A. C. M. Correia, M. Le Feuvre, J. Laskar, and N. Rambaux (2012),
741 Mercury's spin–orbit resonance explained by initial retrograde and subsequent synchronous
742 rotation, *Nature Geosci.*, *5,* 18–21, doi:10.1038/ngeo1350.
743 Wilson, L., and J. W. Head (2008), Volcanism on Mercury: A new model for the history of
744 magma ascent and eruption, *Geophys. Res. Lett.*, *35*, L23205, doi:10.1029/2008GL035620.
745 Wood, C. A. and J. W. Head (1976), Comparison of impact basins on Mercury, Mars, and the
746 Moon, *Proc. Lunar Plan. Sci. Conf., 7th*, 3629–3651.
747 Woronow, A., R. Strom, and M. Gurnis (1982), Interpreting the cratering record: Mercury to
748 Ganymede and Callisto, in *Satellites of Jupiter,* edited by D. Morrison and M. S. Matthews,
749 pp. 237–276, University of Arizona Press, Tuscon, Ariz.
750 Zhong, S. and M. T. Zuber (2000), Long-wavelength topographic relaxation for self-gravitating
751 planets and implications for the time-dependent compensation of surface topography. *J.*
752 *Geophys. Res.*, *105*, 4153–4164.
753 Zuber, M. T., et al. (2012), Topography of the northern hemisphere of Mercury from
754 MESSENGER laser altimetry, *Science*, *336*, 217–220, doi:10.1126/science.1218805.

755

756 D. M. H. Baker and J. W. Head, Department of Geological Sciences, Brown University,
757 Providence, RI 02912, USA
758 C. I. Fassett, Department of Astronomy, Mount Holyoke College, South Hadley, MA 01075,
759 USA. (cfassett@mtholyoke.edu)
760 C. Klimczak and S. C. Solomon, Department of Terrestrial Magnetism, Carnegie Institution of
761 Washington, Washington, DC 20015, USA.
762 G. A. Neumann and D.E. Smith, NASA Goddard Space Flight Center, Greenbelt, MD 20771,
763 USA.
764 J. Oberst and F. Preusker, Institute of Planetary Research, German Aerospace Center, D-
765 12489 Berlin, Germany.
766 R. J. Phillips, Department of Space Sciences, Southwest Research Institute, Boulder, CO
767 80302, USA.
768 L. M. Prockter, The Johns Hopkins University Applied Physics Laboratory, Laurel, MD

20723, USA.

R. G. Strom, Lunar and Planetary Laboratory, University of Arizona, Tucson, AZ 85721, USA.

M. T. Zuber, Department of Earth, Atmospheric, and Planetary Sciences, Massachusetts Institute of Technology, Cambridge, MA 02139-4307, USA.

Figure Captions

Figure 1. Certain (solid white) and probable (dashed white) impact basins on Mercury determined from MESSENGER data, superposed on a global mosaic of MDIS images in the southern hemisphere and MLA topography in the northern hemisphere. (a) Global view in equidistant cylindrical projection; 180° central longitude. (b) North polar region. (c) South polar region. Polar views are polar stereographic projections with lines of longitude and latitude shown in 30° increments.

Figure 2. *R*-plot of the spatial density of large craters and basins for all of Mercury, updated with orbital data from *Fassett et al.* [2011], compared with the Moon. The *R*-plot normalizes the differential size-frequency distribution by a power law of slope -3, so within a count region of area *A,* for *n* craters in the size bin from diameter *a* to diameter *b*, $R=d^3n/A(b-a)$, where *d* is the geometric mean of *a* and *b* [see *Crater Analysis Techniques Working Group*, 1978]. *R* is a measure of areal density, so the larger the value of *R*, the greater the age of the surface, at least if craters are not in saturation equilibrium. This plot is binned by diameter increments of a factor of $\sqrt{2}$ until D = 512 km, above which the diameter increment is a factor of 2 for the largest two bins (D = 512–1024 km and D =1024–2048 km). Errors shown for each point are from counting statistics alone ($R/\sqrt{n}$). Basin diameters are determined on the basis of their inferred topographic rim, equivalent to the Cordillera ring around the lunar Orientale basin. For fresh basins on both the Moon and Mercury, this rim is commonly expressed as an inward facing topographic scarp. The Moon and Mercury are similar in crater density for D =128–512 km, but above D = 512 km there are fewer basins per area on Mercury than the Moon.

Figure 3. 730-km-diameter basin (b36) centered at 7.6°S, 21.6°E. The basin is superposed by a number of peak-ring basins, including the fresh peak-ring basin Derain (white arrow). A lobate scarp is apparent near the southern rim of the basin (bordered arrow).

Figure 4. 470-km-diameter basin (b33) centered at 72.9°S, 149.9°E. This is a degraded basin at high latitudes in the southern hemisphere. The most prominent portion of the basin rim is to the south and west (white arrows); a prominent lobate scarp is to the south and east (bordered arrows).

Figure 5. 470-km-diameter basin (b38) centered at 13.4°S, -6.6°E. This relatively well-preserved basin has prominent radial troughs or basin sculpture to its north, northeast, and east (white arrows) and is floored by smooth plains. A lobate scarp on the basin's eastern margin (bordered arrows) deforms two relatively fresh large craters, 20 km and 40 km in diameter; another scarp is seen on the southern edge of the basin (bordered arrows). There are several secondary crater chains superposed on the basin floor.

Figure 6. 430-km-diameter basin (b37) centered at 27.3°S, -3.2°E. This basin has two large craters superposed on its northern and western rim. Both the basin and these superposed craters have smooth plains on their floors. The crater superposed on the western rim has a lobate scarp (small bordered arrow) in its interior that appears to have been controlled by the earlier basin structure.

Figure 7. 310-km-diameter basin (b40) centered at 6.5°N, 134.8°E. An example of one of the most heavily modified impact basins on Mercury, exposed here as a wrinkle-ridge ring. The basin itself is nearly entirely buried by plains, with the partial exception of its southern rim; sculptured ejecta deposits from Caloris superposed on massifs in its interior (part of a younger crater rim; bordered arrow) indicate that this basin predates the Caloris basin.

Figure 8. Density $N(20)$ of younger craters greater than or equal to 20 km in diameter on basin deposits and interior smooth plains at Caloris, Rembrandt, Beethoven, and Sobkou basins. These data illustrate the separation in time that generally exists between basin formation and the last major volcanism within the basins. Errors shown are from counting statistics alone ($\sqrt{N}/A$).

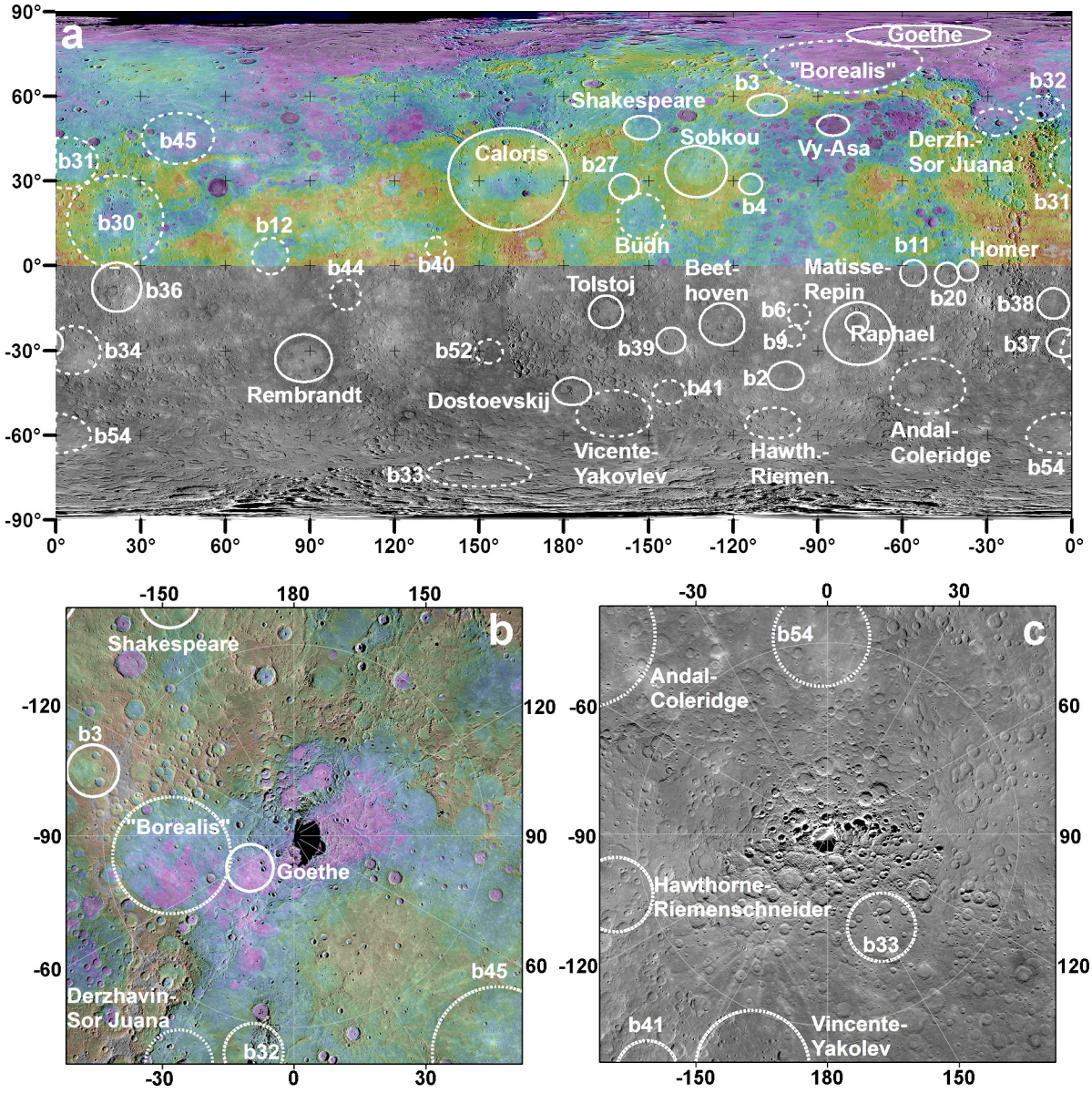
a
Goethe
"Borealis"
b3
b32
Shakespeare
Sobkou
Vy-Asa
Derzh.-
Sor Juana
b45
b31
Caloris
b27
b4
b31
b30
b12
Budh
b11
Homer
b44
b40
Tolstoj
Beet-
hoven
Matisse-
Repin
b20
b38
b36
b6
b34
b52
b39
b9
Raphael
b37
Rembrandt
Dostoevskij
b41
b2
b54
Andal-
Coleridge
Vicente-
Yakovlev
Hawth.-
Riemen.
b33
b54
90°
60°
30°
0°
-30°
-60°
-90°
0°
30°
60°
90°
120°
150°
180°
-150°
-120°
-90°
-60°
-30°
0°
b
Shakespeare
b3
"Borealis"
Goethe
b45
Derzhavin-
Sor Juana
b32
-150
180
150
-120
-90
-60
120
90
60
-30
0
30
c
b54
Andal-
Coleridge
Hawthorne-
Riemenschneider
b33
b41
Vincente-
Yakolev
-30
0
30
-60
-90
-120
60
90
120
-150
180
150

Figure 1

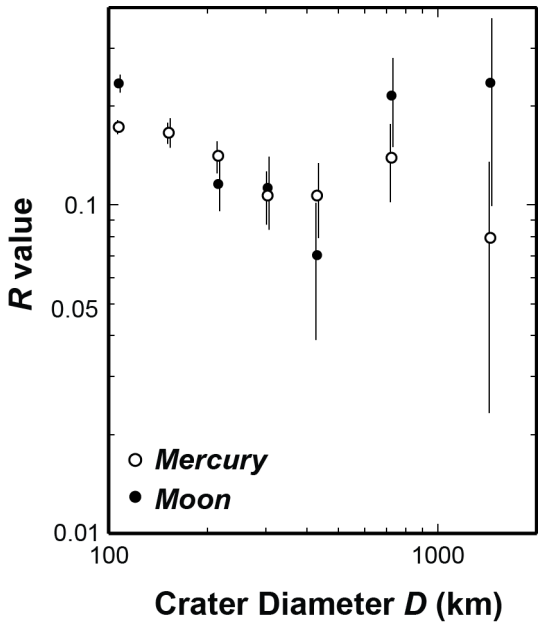

Figure 2

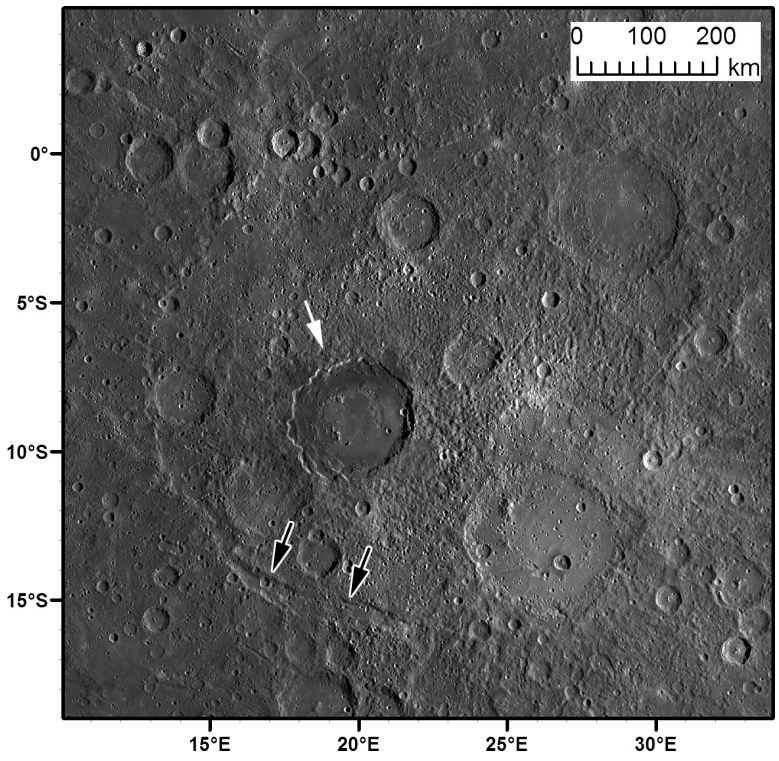

Figure 3

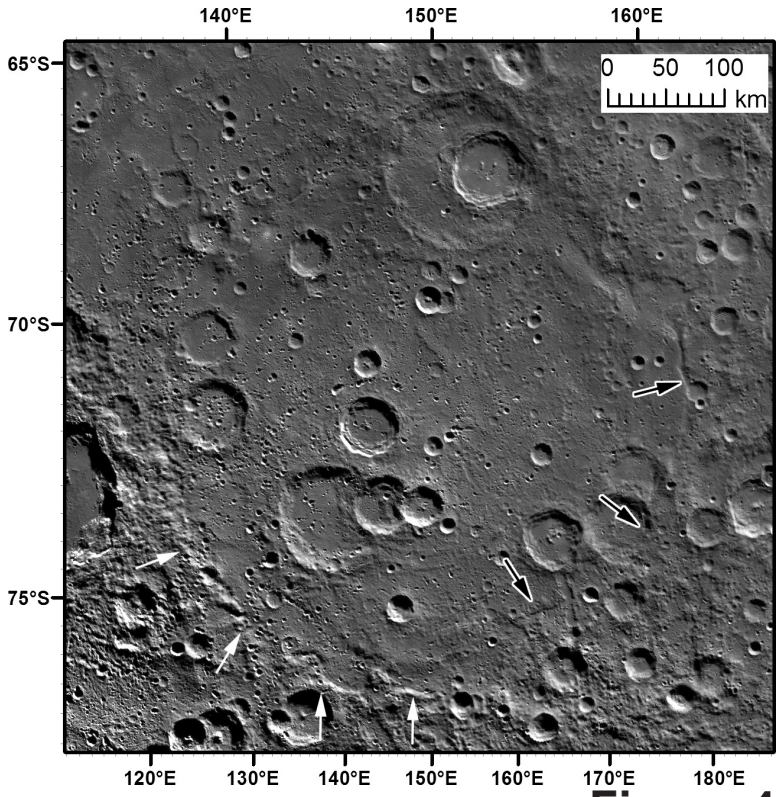

Figure 4

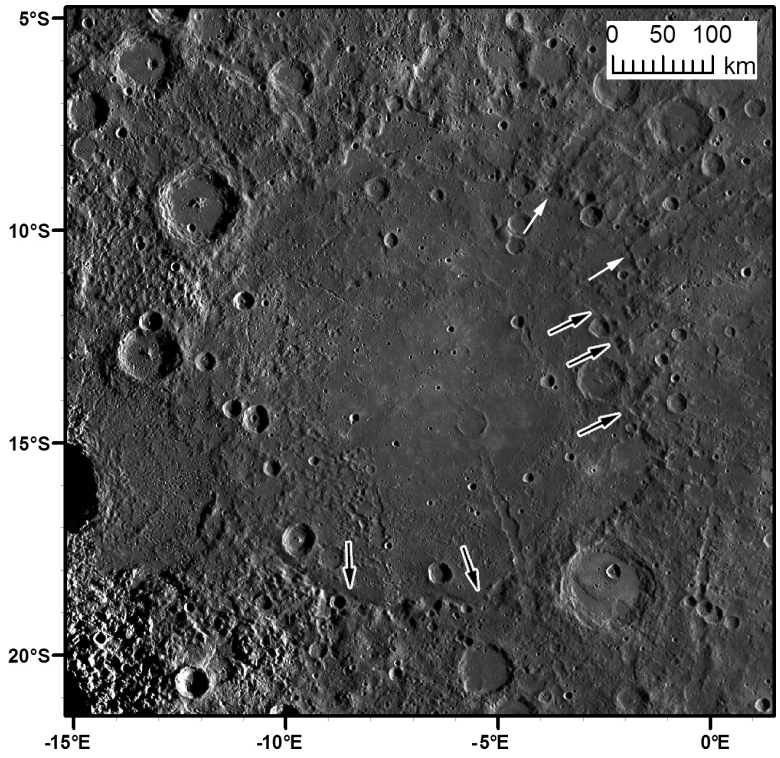

Figure 5

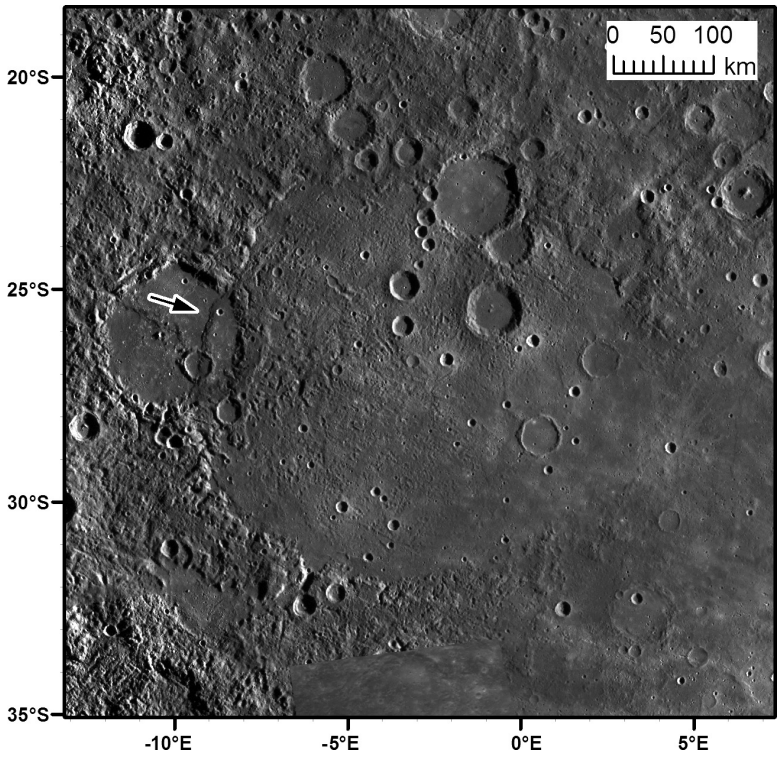

Figure 6

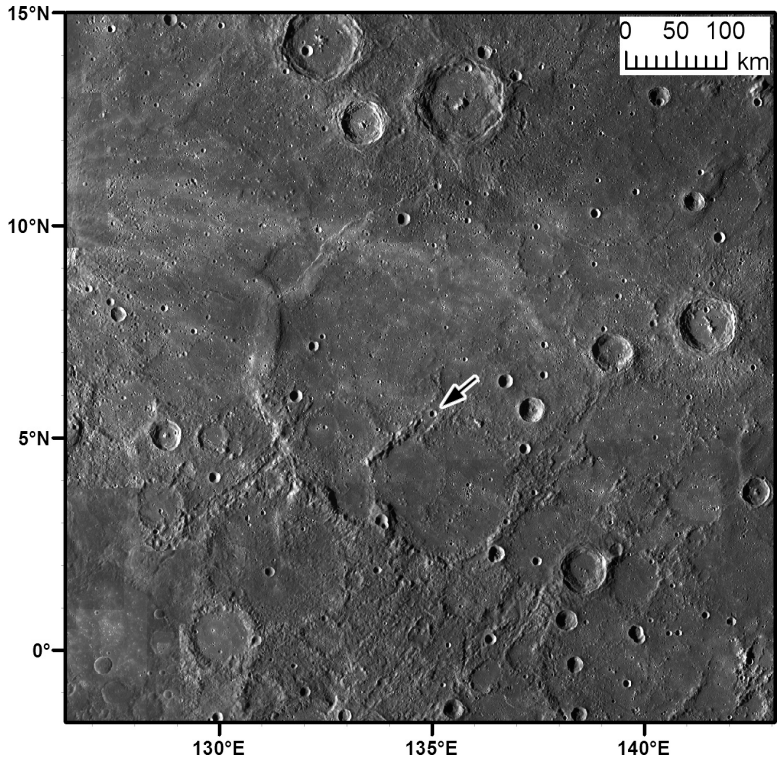

Figure 7

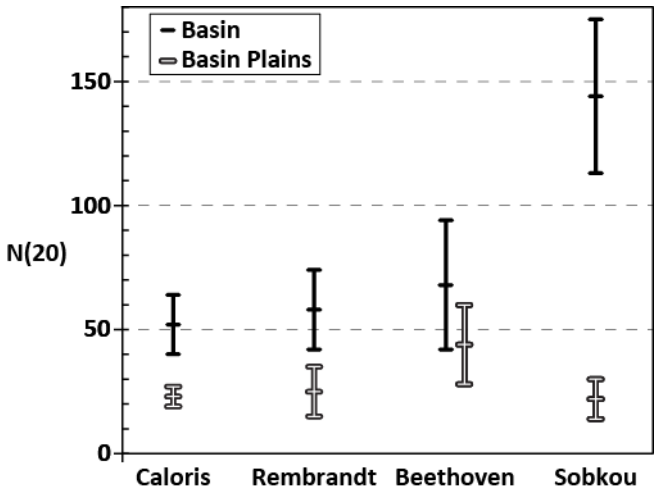
Basin
Basin Plains
150
100
50
0
N(20)
Caloris
Rembrandt
Beethoven
Sobkou

Figure 8